

# NON-HYDROSTATIC FLOW SIMULATION USING THE FILLY NONLINEAR WEAKLY DISPERSIVE SERRE EQUATIONS

Christopher Zoppou,<sup>1</sup> Member, ASCE  
Stephen G. Roberts,<sup>1</sup> Not a Member, ASCE

## ABSTRACT

The shallow water wave equations assume a hydrostatic pressure distribution. Large surface gradients in free surface flow will produce flows that have a non-hydrostatic pressure distribution. Nonlinear equations that describe these flows contain dispersive terms. The nonlinear and weakly dispersive Serre equations contain higher-order dispersive terms. This includes a mixed spatial and temporal derivative flux term which is difficult to handle numerically. We replace this term by a new conserved quantity which facilitates the use of standard techniques for solving the shallow water wave equations for the solution of the Serre equations. The remaining primitive variable is obtained by solving a second-order elliptic equation. We describe how this is achieved. The advantage of this approach is that problems with steep gradients can now be solved without assuming a hydrostatic pressure distribution. Using analytical solutions, laboratory flume data and by simulating the dam-break problem, we demonstrate the importance of including dispersion terms in simulation rapidly varying flows by comparing the results from the solution of the Serre equations with the results from the solution of the shallow water wave equations. Our approach is accurate, stable and only slightly more expensive than solving the shallow water wave equations.

**Keywords:** dispersive waves, conservation laws, Serre equation, shallow waster wave equations, finite volume method

## <sup>1</sup> INTRODUCTION

Rapidly-varying free surface flows are characterized by large surface gradients. These flows can be found for example, in hydraulic jumps, tsunamis, tidal bores and releases from power stations. Large surface gradients produce vertical accelerations of fluid particles and a non-hydrostatic pressure distribution.

System of equations that describe the behaviour of these flows are obtained from the three-dimensional Euler equations for incompressible flows with constant density. By integrating the Euler equations over the water depth results in system of equations that are

---

<sup>1</sup>Mathematical Sciences Institute, Australian National University, Canberra, ACT 0200, Australia, E-mail: Christopher.Zoppou@anu.edu.au. The work undertaken by the first author was supported financially by an Australian National University Postgraduate Research Award.

more amenable for efficient solution by numerical techniques and suitable for solving practical problems. If non-hydrostatic pressure distribution is assumed, one arrives at a system of equations that contain dispersive terms. If the hydrostatic assumption is assumed, then the shallow water wave equations are obtained, which ignore dispersive terms.

Systems of equations that contain nonlinear and dispersive terms are known as Boussinesq-type equations. There is, however, no unique Boussinesq-type equation. Different derivation approaches and the order of accuracy of the terms retained in the derivation results in a variety of equations with different dispersion characteristics (Madsen et al. 1991). Some models are based on primitive variables (Shiach and Mingham 2009).

The validity of the various equation systems is still being debated. However, all require that the water depth  $h_0 \ll L \sim 1/k$  is much smaller than the horizontal wave length,  $L$ , and  $k$  is the wave number. The range of validity of these equations is dependent on the nonlinearity parameter,  $\epsilon = a/h_0$ , where  $a$  is a typical wave amplitude. The Boussinesq wave theory requires the shallowness  $\sigma = h_0^2/L^2 \sim \epsilon \ll 1$ .

In contrast to some Boussinesq-type equations, which rely on small amplitude theory, the fully nonlinear and weakly dispersive Serre equations can be derived directly from the free surface Euler equations. There is no restriction on  $\epsilon$  for the Serre equations (Li 2006). Therefore, the Serre equations are applicable up to wave breaking where  $\epsilon \sim O(1)$  (Barthélemy 2004). Bonneton *et al.* (Bonneton et al. 2011b; Bonneton et al. 2011a) consider the weakly dispersive fully nonlinear Serre equations as the most appropriate system to model dispersive waves at the shoreline.

Finite-difference schemes have been the most popular method for solving nonlinear dispersive equations (Antunes do Carmo et al. 1993; Nwogu 1993; El et al. 2008; Beji and K. Nadaoka 1996). Finite-element techniques (Avilez-Valente and Seabra-Santos 2009; Mitsotakis 2009) and spectral methods (Dias and Milewski 2010; Eskilsson and Sherwin 2002) have also been employed. More recently, the finite volume method (Shiach and Mingham 2009; Erduran et al. 2005; Erduran 2007; Soares-Frazão and Guinot 2008; Tonelli and Petti 2012; Roeber et al. 2010; Tonelli and Petti 2009) has become popular.

A major difficulty with solving some Boussinesq-type and the Serre equations, it that the dispersive terms contain a mix spatial and temporal derivative term (Dias and Milewski 2010). In many instances operator splitting techniques have been employed where standard shock capturing techniques are used to solve the shallow water wave equations and an implicit or semi-implicit finite difference scheme is used to solve the stiff source term, which contain the dispersive terms (Shiach and Mingham 2009; Bonneton et al. 2011a; Erduran 2007; Soares-Frazão and Guinot 2008; Tonelli and Petti 2009; Chazel et al. 2011). Alternatively, a predictor-corrector strategy, involving iteration is usually required to solve the equations because of the mixed derivative dispersive term (Beji and K. Nadaoka 1996; Erduran 2007; Roeber et al. 2010; Shi et al. 2012).

47 A finite volume technique is proposed for the solution of the fully nonlinear and weakly  
 48 dispersive Serre equations without the need for iteration or operator splitting. This is  
 49 achieved by replacing the mix spatial and temporal derivative term in the flux term by a  
 50 combination of temporal and spatial terms so that the Serre equations can be written in  
 51 conservation law form. The final system of equations contains a new conserved quantity  
 52 and its corresponding flux term. Standard techniques that are applied to solve nonlinear  
 53 conservation laws, such as the shallow water wave equations can be used to solve the Serre  
 54 equation for the new conserved quantities. The remaining primitive variable is obtained  
 55 by solving a second-order elliptic equation.

56 The performance of the proposed finite volume scheme for solving the conservative  
 57 form of the Serre equations is evaluated with the help of an analytical solution to the Serre  
 58 equations, laboratory flume data and the simulation of the dam-break problem. With the  
 59 exception of the analytical solution, which is smooth, the remaining problems involve the  
 60 simulation of discontinuities that produce dispersive waves.

61 The consequences of assuming a hydrostatic pressure distribution for rapidly varying  
 62 flows is demonstrated by comparing the results from the solution of the Serre equations  
 63 with the results from solving the shallow water wave equations using laboratory flume data  
 64 and the dam-break problem.

65 In the next section we provide a brief derivation of the standard Serre equations from  
 66 the Euler equations. In Section 3, the Serre equations are written in terms of the new  
 67 conserved quantities and we provide justification for writing the Serre equations in this  
 68 form. The properties of the linearized form of the Serre equation are examined in Section  
 69 3. The second-order solution of the Serre equations written in terms of the new conserved  
 70 quantity is described in detail in Section 4. In Section 4, the numerical schemes is also  
 71 validated using an analytical solution. Using laboratory flume data and the simulation of  
 72 the dam-break problem, the consequences of assuming a hydrostatic pressure distribution  
 73 for rapidly varying flows is demonstrated by comparing the results from the solution of the  
 74 Serre equations with the results from solving the shallow water wave equations in Section  
 75 5. Finally, conclusions are drawn and presented in Section 6

## 76 **SERRE EQUATIONS**

77 For an invicid free-surface incompressible fluid with constant density,  $\rho$  the conserva-  
 78 tion of mass and momentum are given by the Euler equations

$$79 \frac{\partial u}{\partial x} + \frac{\partial w}{\partial z} = 0, \quad (1a)$$

$$82 \frac{\partial u}{\partial t} + u \frac{\partial u}{\partial x} + w \frac{\partial u}{\partial z} = -\frac{1}{\rho} \frac{\partial p}{\partial x}, \quad (1b)$$

84 and

85                    86

$$\frac{\partial w}{\partial t} + u \frac{\partial w}{\partial x} + w \frac{\partial w}{\partial z} = -\frac{1}{\rho} \frac{\partial p}{\partial z} - g, \quad (1c)$$

87 in two planar dimensions,  $\mathbf{x} = (x, z)$ . Consider a fluid particle at depth  $\xi = z - h - z_b$   
88 below the water surface, see Figure 1, where the water depth is  $h(x, t)$  and  $z_b(x)$  is the bed  
89 elevation. The fluid particle is subject to the pressure,  $p(\mathbf{x}, t)$  and gravitational acceleration,  
90  $\mathbf{g} = (0, g)^T$  and has a velocity  $\mathbf{u} = (u(\mathbf{x}, t), w(\mathbf{x}, t))$ , where  $u(\mathbf{x}, t)$  is the velocity in the  $x$ -  
91 coordinate and  $w(\mathbf{x}, t)$  is the velocity in the  $z$ -coordinate and  $t$  is time. In addition to the  
92 above equations, a number of boundary conditions must be satisfied. These are;

- 93                    • the kinematic condition at the free surface ( $z = h + z_b$ ),

96

$$w|_{h+z_b} = \frac{\partial h}{\partial t} + u \frac{\partial(h + z_b)}{\partial x}, \quad (2a)$$

- 98                    • the kinematic condition at the bed ( $z = z_b$ )

100

$$w|_{z_b} = u \frac{\partial z_b}{\partial x}, \quad (2b)$$

- 102                    • the dynamic condition at the surface ( $z = h + z_b$ )

103

$$p(\xi = 0) = p_a. \quad (2c)$$

105 This is the atmospheric pressure at the water surface, usually taken to be  $p_a = 0$ .

106 The three-dimensional problem can be reduced to a two-dimensional problem in  $(x, y)$   
107 by incorporating the vertical velocity of the fluid particles with additional higher-order  
108 terms in the  $x$ - and  $y$ -momentum equations. For example, in the  $x$ -direction, this can be  
109 achieved by choosing the horizontal velocity variable,  $u(x, z, t)$  or the functional form of  
110 the variation of  $u(x, z, t)$  with depth. The choice of horizontal velocity variable,  $u(x, z, t)$   
111 to be used, results in a variety of equations with different forms and different dispersion  
112 characteristics (Madsen et al. 1991; Beji and K. Nadaoka 1996; Madsen and Sørensen  
113 1992; Witting 1984; Zou 1999). It has been shown by Mei et al. (2005) and Nwogu (1993)  
114 that the accuracy of linear dispersion characteristics is dependent on the choice of the  
115 velocity variable. The choice of velocity variable is not unique. In the derivation of the  
116 Serre equation, instead of using the velocity at a particular depth, the point velocity in the  
117  $x$ -direction is assumed to be uniform over the water depth, so that  $u(x, z, t) = \bar{u}(x, t)$ . This  
118 assumption is not necessary for the derivation of the continuity equation. If the depth-

averaged velocity in the  $x$ -direction, given by

$$\bar{u} = \frac{1}{h} \int_{z_b}^{h+z_b} u(x, z, t) dz$$

<sup>122</sup> is used, then the continuity equation

$$\frac{\partial h}{\partial t} + \bar{u} \frac{\partial h}{\partial x} + h \frac{\partial \bar{u}}{\partial x} = 0 \quad (3)$$

125 where  $h$  and  $\bar{u}$  are the primitive variables, is exact.

From (1a) it follows that the vertical velocity at any depth  $z - z_b$  is given by

$$w|_z = -(z - z_b) \frac{\partial \bar{u}}{\partial x} \quad (4)$$

for a horizontal bed. The vertical velocity is a linear function of the water depth, zero at the bed and a maximum at the water surface. The shallow water wave equations assume that  $w|_{\zeta} = 0$ .

Integrating the point quantities in (1b) over the flow depth  $z_b$  to  $h + z_b$ , and satisfying (2) produces the one-dimensional  $x$ -momentum equations

$$\frac{\partial \bar{u}}{\partial t} + \bar{u} \frac{\partial \bar{u}}{\partial x} + \frac{1}{h} \frac{\partial}{\partial x} \left[ \frac{gh^2}{2} + \frac{h^3}{3} \left( \frac{\partial \bar{u}}{\partial x} \frac{\partial \bar{u}}{\partial x} - \bar{u} \frac{\partial^2 \bar{u}}{\partial x^2} - \frac{\partial^2 \bar{u}}{\partial x \partial t} \right) \right] = 0 \quad (5)$$

136 Equation (5) contain a third-order spatial derivative term and has the form of a dispersion  
137 equation. This term can severely restrict the time step that can be used if standard explicit  
138 finite difference schemes are used to solve these equations.

Multiplying (5) by  $h$ , adding (3) pre-multiplied by  $\bar{u}$  and making use of (3) to obtain;

$$\frac{\partial h}{\partial t} + \frac{\partial(\bar{u}h)}{\partial x} = 0 \quad (6a)$$

142 and

$$\underbrace{\frac{\partial(\bar{u}h)}{\partial t} + \frac{\partial}{\partial x}\left(\bar{u}^2h + \frac{gh^2}{2}\right)}_{\text{Shallow Water Wave Equations}} + \underbrace{\frac{\partial}{\partial x}\left(\frac{h^3}{3}\left[\frac{\partial\bar{u}}{\partial x}\frac{\partial\bar{u}}{\partial x} - \bar{u}\frac{\partial^2\bar{u}}{\partial x^2} - \frac{\partial^2\bar{u}}{\partial x\partial t}\right]\right)}_{\text{Dispersion Terms}} = 0. \quad (6b)$$

Serre Equations

<sup>145</sup> which is written in terms of the conservative variables,  $h$  and  $\bar{u}h$ . The terms in the square  
<sup>146</sup> parenthesis are the dispersive terms which contain high order spatial derivative terms and a

147 mixed spatial and temporal derivative term. This is generally the case for dispersive equa-  
 148 tions, with the exception of the Boussinesq equation (Basco 1987), where the momentum  
 149 equation is given by

$$150 \quad \frac{\partial(\bar{u}h)}{\partial t} + \frac{\partial}{\partial x} \left( \bar{u}^2 h + \frac{gh^2}{2} \right) - \frac{h^3}{3} \frac{\partial^3 \bar{u}}{\partial x^2 \partial t} = 0. \quad (7)$$

152 the product derivative and third-order space derivative terms in (6b) are ignored.

153 The dispersive terms influence the pressure distribution in the water column, which is  
 154 given by

$$155 \quad p|_{\xi} = p_a + \rho g \xi + \frac{\rho}{2} \xi (2h - \xi) \left( \frac{\partial \bar{u}}{\partial x} \frac{\partial \bar{u}}{\partial x} - \bar{u} \frac{\partial^2 \bar{u}}{\partial x^2} - \frac{\partial^2 \bar{u}}{\partial x \partial t} \right). \quad (8)$$

157 It is less than the hydrostatic pressure,  $p(\xi) = \rho g \xi$  at the crest of a wave and greater than  
 158 the hydrostatic pressure distribution at the troughs. Ignoring all the dispersive terms in  
 159 (6b) results in the well known nonlinear shallow water wave equations, where the pressure  
 160 distribution is hydrostatic.

161 Equation (6) are known as the Serre equations (Serre 1953; Seabra-Santos et al. 1981;  
 162 Carter and Cienfuegos 2011) and unlike some Boussinesq-type equations, they retain full  
 163 nonlinearity in the dispersive terms (El et al. 2006). They have been derived by Serre  
 164 (Serre 1953), Su and Gardner (Su and Gardner 1969) and Seabra-Santos *et al.* (Seabra-  
 165 Santos et al. 1981) and are equivalent to the depth averaged Green and Naghdi (Green and  
 166 Naghdi 1976) equations. They are considered to be good approximations to the full Euler  
 167 equations up to a wave breaking (Bonneton et al. 2011b; Bonneton et al. 2011a). Unlike  
 168 the shallow water wave equations, which are hyperbolic for finite water depth, although  
 169 they are evolution-type equations, the Serre equations are neither hyperbolic or parabolic.

170 The major differences between the Serre and shallow water wave equations are sum-  
 171 marized in Table 2.

## 172 ALTERNATIVE CONSERVATION LAW FORM OF THE SERRE EQUATIONS

173 We could solve the Serre equations using a variety of methods. However, if we can  
 174 write the equations in conservation law form, then there are very efficient schemes for solv-  
 175 ing conservation laws which could be used to solve the Serre equations. These schemes  
 176 are capable of handling step gradients in a problem with potentially a significant saving in  
 177 computational effort if the Serre equations can be written in conservation law form.

178 For example, using a simple explicit finite difference schemes, stability analysis of sim-  
 179 ple explicit finite differences scheme for the advection equation (conservation law form)

$$180 \quad \frac{\partial q}{\partial t} + \frac{\partial q}{\partial x} = 0, \quad \Delta t \leq \Delta x$$

182 would show that the computational time step is proportional to the computation distance  
 183 step. For the diffusion equation

$$184 \quad \frac{\partial q}{\partial t} - \frac{\partial^2 q}{\partial x^2} = 0, \quad \Delta t \leq \Delta x^2 / 2 \\ 185$$

186 the computational time step is proportional to  $\Delta x^2$  and for the dispersion equation

$$187 \quad \frac{\partial q}{\partial t} + \frac{\partial^3 q}{\partial x^3} = 0 \quad \Delta t \leq \Delta x^3 / 2 \\ 188$$

189 the time step is proportional to  $\Delta x^3$ . Potentially there is considerable savings to be made  
 190 if the Serre equations can be written in conservation law form.

191 The flux term in the momentum equation, (6b) contains a mixed spatial and temporal  
 192 derivative term which is difficult to treat numerically. It is possible to replace this term by  
 193 a combination of spatial and temporal derivative terms.

194 Consider

$$195 \quad \frac{\partial^2}{\partial x \partial t} \left( \frac{h^3}{3} \frac{\partial \bar{u}}{\partial x} \right) = \frac{\partial}{\partial t} \left( h^2 \frac{\partial h}{\partial x} \frac{\partial \bar{u}}{\partial x} + \frac{h^3}{3} \frac{\partial^2 \bar{u}}{\partial x^2} \right) = \frac{\partial}{\partial x} \left( h^2 \frac{\partial h}{\partial t} \frac{\partial \bar{u}}{\partial x} + \frac{h^3}{3} \frac{\partial^2 \bar{u}}{\partial x \partial t} \right). \\ 196$$

197 Rearranging then

$$198 \quad \frac{\partial}{\partial x} \left( \frac{h^3}{3} \frac{\partial^2 \bar{u}}{\partial x \partial t} \right) = \frac{\partial}{\partial t} \left( h^2 \frac{\partial h}{\partial x} \frac{\partial \bar{u}}{\partial x} + \frac{h^3}{3} \frac{\partial^2 \bar{u}}{\partial x^2} \right) - \frac{\partial}{\partial x} \left( h^2 \frac{\partial h}{\partial t} \frac{\partial \bar{u}}{\partial x} \right). \\ 199$$

200 Making use of the continuity equation, (6a)

$$201 \quad \frac{\partial}{\partial x} \left( \frac{h^3}{3} \frac{\partial^2 \bar{u}}{\partial x \partial t} \right) = \frac{\partial}{\partial t} \left( h^2 \frac{\partial h}{\partial x} \frac{\partial \bar{u}}{\partial x} + \frac{h^3}{3} \frac{\partial^2 \bar{u}}{\partial x^2} \right) + \frac{\partial}{\partial x} \left[ h^2 \frac{\partial \bar{u}}{\partial x} \left( \bar{u} \frac{\partial h}{\partial x} + h \frac{\partial \bar{u}}{\partial x} \right) \right] \\ 202$$

203 and the momentum equation, (6b) becomes

$$204 \quad \frac{\partial}{\partial t} \left( \bar{u}h - h^2 \frac{\partial h}{\partial x} \frac{\partial \bar{u}}{\partial x} - \frac{h^3}{3} \frac{\partial^2 \bar{u}}{\partial x^2} \right) + \frac{\partial}{\partial x} \left( \bar{u}^2 h + \frac{gh^2}{2} - \bar{u}h^2 \frac{\partial h}{\partial x} \frac{\partial \bar{u}}{\partial x} - \frac{\bar{u}h^3}{3} \frac{\partial^2 \bar{u}}{\partial x^2} - \frac{2h^3}{3} \frac{\partial \bar{u}}{\partial x} \frac{\partial \bar{u}}{\partial x} \right) = 0. \\ 205$$

206 The momentum equation can be written in terms of a new conservative quantity as

$$207 \quad \frac{\partial G}{\partial t} + \frac{\partial}{\partial x} \left( G \bar{u} + \frac{gh^2}{2} - \frac{2h^3}{3} \frac{\partial \bar{u}}{\partial x} \frac{\partial \bar{u}}{\partial x} \right) = 0 \quad (9) \\ 208$$

209 where the new conserved quantity,  $G$  is given by the second-order elliptic equation

$$210 \quad G = \bar{u}h - h^2 \frac{\partial h}{\partial x} \frac{\partial \bar{u}}{\partial x} - \frac{h^3}{3} \frac{\partial^2 \bar{u}}{\partial x^2} \quad (10) \\ 211$$

212 which can be written in divergent form as

$$213 \quad G = \bar{u}h - \frac{\partial}{\partial x} \left( \frac{h^3}{3} \frac{\partial \bar{u}}{\partial x} \right). \quad (11)$$

214

215 The temporal derivative in the momentum equation has been eliminated from the flux term.  
 216 In contrast to (6), the flux term now only contains spatial derivatives. The quantity,  $G/h$   
 217 is known as irrotationality (Carter and Cienfuegos 2011) or potential vorticity (Dias and  
 218 Milewski 2010). The quantity  $G$  is a new conserved variable that is admissible to the Serre  
 219 equation. The Serre equations also admit the conservation of mass, momentum, energy  
 220 and irrotationality (Bonneton et al. 2011b; Carter and Cienfuegos 2011). For smooth  
 221 problems, all of these equations and (9) will produce identical solutions.

222 The alternative form of the Serre equations can be written in vector form as

$$223 \quad \frac{\partial \mathbf{U}(x, t)}{\partial t} + \frac{\partial \mathbf{F}(\mathbf{U}(x, t))}{\partial x} = 0. \quad (12a)$$

224

225 where,

$$226 \quad \mathbf{U}(x, t) = \begin{bmatrix} h \\ G \end{bmatrix}, \quad (12b)$$

227

228 and

$$229 \quad \mathbf{F}(\mathbf{U}(x, t)) = \begin{bmatrix} f(1) \\ f(2) \end{bmatrix} = \begin{bmatrix} \bar{u}h \\ G\bar{u} + \frac{gh^2}{2} - \frac{2h^3}{3} \frac{\partial \bar{u}}{\partial x} \frac{\partial \bar{u}}{\partial x} \end{bmatrix}. \quad (12c)$$

230

### 231 Properties of the modified Serre equations

232 The Serre equations have two identical pairs of characteristics with slopes

$$233 \quad \frac{dx}{dt} = \bar{u}, \bar{u} \quad \text{and} \quad \frac{dx}{dt} = \infty, \infty.$$

234

235 They are not hyperbolic and do not have any Riemann invariants. However, useful prop-  
 236 erties of the Serre equations, (6) or (12) can be obtained by applying the Fourier analysis  
 237 to the linearized equations and observing the behaviour of a harmonic wave of the form

$$238 \quad h(x, t) = A e^{i(kx - \omega t)} \quad \text{and} \quad u(x, t) = U e^{i(kx - \omega t)} \quad (13)$$

240 where  $A$  and  $U$  are unknown coefficients,  $\omega$  is the frequency,  $k$  the wave number and  
 241  $i = \sqrt{-1}$ .

242 The linearized Serre equations are obtained by assuming that the solution of  $\bar{u}(x, t)$  and  
 243  $h(x, t)$  can be expressed as

$$244 \quad h(x, t) = h_0(x, t) + \epsilon h_1(x, t) + \epsilon^2 h_2(x, t) + \dots \quad (14a)$$

246 and

$$247 \quad \bar{u}(x, t) = u_0(x, t) + \epsilon u_1(x, t) + \epsilon^2 u_2(x, t) + \dots \quad (14b)$$

249 where  $u_0, u_1, \dots, h_0, h_1, \dots$  are to be determined.

250 Using (14), then the continuity equation, (6a) becomes, to terms of up to order  $\epsilon$

$$251 \quad 252 \quad \frac{\partial h_1}{\partial t} + h_0 \frac{\partial u_1}{\partial x} + u_0 \frac{\partial h_1}{\partial x} = 0 \quad (15a)$$

253 and for the momentum equation, (6b)

$$254 \quad 255 \quad \frac{\partial u_1}{\partial t} + g \frac{\partial h_1}{\partial x} + u_0 \frac{\partial u_1}{\partial x} - \frac{h_0^2}{3} \left( u_0 \frac{\partial^3 u_1}{\partial x^3} + \frac{\partial^3 u_1}{\partial x^2 \partial t} \right) = 0 \quad (15b)$$

256 which makes use of the linearized continuity equation.

257 Substituting (13), the linearized equations become

$$258 \quad -A\omega + u_0Ak + h_0Uk = 0, \quad (16a)$$

260 and

$$261 \quad 262 \quad -U\omega + gAk + u_0Uk - \frac{1}{3}h_0^2U\omega k^2 + \frac{1}{3}h_0^2u_0Uk^3 = 0. \quad (16b)$$

263 For a nontrivial solution

$$264 \quad 265 \quad \begin{vmatrix} -\omega + u_0k & h_0k \\ gk & -\omega + u_0k - \frac{1}{3}h_0^2\omega k^2 + \frac{1}{3}h_0^2u_0k^3 \end{vmatrix} = 0$$

266 or

$$267 \quad 268 \quad \omega_{1,2} = u_0k \pm k \sqrt{gh_0} \sqrt{\frac{3}{\mu^2 + 3}}$$

269 where  $\mu = h_0k$  is the frequency dispersion. The dispersive terms have no effect on  $u_0$ , only  
 270 on the celerity of a small disturbance.

271 For non-dispersive waves, the phase velocity,  $v_p = \text{Re}(\omega)/k$  is identical to the group  
 272 velocity  $v_g = d\text{Re}(\omega)/dk$ . This is the case for the shallow water wave equation where,  
 273  $v_p = v_g = u_0 \pm \sqrt{gh_0}$ . The phase speed is independent of the wave number,  $k$  and all  
 274 wave components travel at the same speed,  $u_0 \pm \sqrt{gh_0}$ . This is not the case for the Serre  
 275 equation, where the phase speed is

$$276 \quad v_p = u_0 \pm \sqrt{gh_0} \sqrt{\frac{3}{\mu^2 + 3}} \quad (17a)$$

277 and the group velocity is

$$279 \quad v_g = u_0 \pm \sqrt{gh_0} \left( \sqrt{\frac{3}{\mu^2 + 3}} \mp \mu^2 \sqrt{\frac{3}{(\mu^2 + 3)^3}} \right) \neq v_p. \quad (17b)$$

281 Both are dependent on the wave number,  $k$ . Since the group speed is slower than the phase  
 282 speed, the Serre equations describe dispersive waves. This is a characteristic of dispersive  
 283 waves, the group and phase speeds differ.

## 284 SOLVING THE SERRE EQUATIONS WRITTEN IN CONSERVATION LAW 285 FORM

286 The Serre equations is solved using a second-order finite volume method. In a finite  
 287 volume method the solution to a conservation law, (12a) is advanced by solving

$$288 \quad \frac{\partial \mathbf{U}_j}{\partial t} + \frac{1}{V_j} \oint_{S_j} \mathbf{F}(\mathbf{U}) \cdot \vec{\mathbf{n}} ds = 0 \quad (18)$$

290 where  $S_j$  is the surface area of element  $I_j$ ,  $V_j$  is the volume of the element  $I_j$  and  $\vec{\mathbf{n}}$  is the  
 291 unit vector normal to the surface of element  $I_j$  pointing outward. In one-dimension, the  
 292 cells are line segments  $I_j = [x_{j-1/2}, x_{j+1/2}]$  that are assumed to be uniform in space. Then  
 293 (18) can be written in semi-discrete form as

$$294 \quad \frac{d\bar{q}_j(t)}{dt} = \mathcal{L}(\bar{q}(x, t)) = \frac{f(\bar{q}(x_{j+1/2}, t)) - f(\bar{q}(x_{j-1/2}, t))}{\Delta x} \quad (19)$$

296 for a conserved quantity,  $q(x, t)$  where  $\Delta x = x_{j+1/2} - x_{j-1/2}$ ,  $x_j = (x_{j+1/2} + x_{j-1/2})/2$ .

297 In the discrete forms of (18),  $f(q(x_{j\pm 1/2}, t)) = f_{j\pm 1/2}(q_{j-1}(t), \dots, q_{j+1}(t)) = F_{j\pm 1/2}$  repre-  
 298 sents the numerical approximation of the physical flux  $f(q(x, t))$  of the conserved quantity,  
 299  $q(x, t)$  across the boundary of cell  $I_j$  at  $x_{j\pm 1/2}$  at time  $t$ , and

$$300 \quad \bar{q}_j(t) = \frac{1}{\Delta x} \int_{x_{j-1/2}}^{x_{j+1/2}} q(x, t) dx \quad (20)$$

302 is the average value of the state variable,  $q(x, t)$  in  $I_j$  at time  $t$ . Equation (20) ensures that  
 303 mass is conserved in each cell.

304 The flux,  $F_{j+1/2}$  is a function of the left and right extrapolated state values  $q_{j+1/2}^+$  and  
 305  $q_{j+1/2}^-$ , obtained from piecewise polynomials passing through consecutive values of  $\bar{q}_j$ .  
 306 Therefore,

$$307 \quad F_{j+1/2} = f_{j+1/2}(q_{j+1/2}^+, q_{j+1/2}^-).$$

309 At the cell interface generally,  $q_{j+1/2}^+ \neq q_{j+1/2}^-$  and a local Riemann problem is solved to  
 310 obtain the flux between the cells.

311 The overall accuracy of the numerical scheme is dependent on the accuracy of the re-  
 312 construction method and the order of accuracy of the time integration of the semi-discrete  
 313 system, (19).

### 314 Reconstruction

315 To achieve second-order,  $O(\Delta x^2)$  accuracy a linear polynomial,  $P_j(x) = a_j + b_j(x - x_j)$   
 316 is fitted through the cell averages. The reconstructed cell interface values are given by

$$317 \quad q_{j+1/2}^- = \bar{q}_j + \phi(r_j) \frac{\bar{q}_j - \bar{q}_{j-1}}{2} \quad (21a)$$

319 and

$$320 \quad q_{j-1/2}^+ = \bar{q}_j - \phi(r_j) \frac{\bar{q}_j - \bar{q}_{j-1}}{2} \quad (21b)$$

322 where

$$323 \quad r_j = \frac{\bar{q}_j - \bar{q}_{j-1}}{\bar{q}_{j+1} - \bar{q}_j} = \frac{\Delta \bar{q}_{j-1/2}}{\Delta \bar{q}_{j+1/2}}$$

325 and  $\phi(r_j)$  is a nonlinear constraints imposed on the reconstruction to ensures that the  
 326 scheme remains TVD and second-order away from extremes, where  $r < 0$ . The nonlinear  
 327 limiter prevents unwanted oscillations and ensures that the results are physical (bounded)  
 328 and therefore stable.

329 An example of a non-linear limiter is the *generalized minmod* limiter (van Leer 1979)

$$330 \quad \phi(\bar{q}, \theta) = \text{minmod}\left(\theta \Delta \bar{q}_{j-1/2}, (\Delta \bar{q}_{j+1/2} + \Delta \bar{q}_{j-1/2})/2, \theta \Delta \bar{q}_{j+1/2}\right), \quad 1 \leq \theta \leq 2,$$

332 where

$$333 \quad \text{minmod}(x_1, x_2, x_3, \dots) = \begin{cases} \min_j(x_j) & \text{if } x_j > 0, \forall j, \\ \max_j(x_j) & \text{if } x_j < 0, \forall j, \\ 0 & \text{otherwise.} \end{cases}$$

334 The parameter  $\theta$  controls the amount of diffusion in the numerical scheme. When a local  
 335 extrema has been encountered,  $r_j \leq 0$  and  $\phi(r_j) = 0$ . In this case the reconstruction reverts  
 336 to a piecewise constant reconstruction. In smooth regions,  $r_j \rightarrow 1$  and  $\phi(r_j) \rightarrow 1$  and the  
 337 reconstruction is first-order producing a second-order accurate scheme.

### 338 Local Riemann Problem

339 The reconstruction of the conserved quantities,  $\bar{q}_{j\pm 1/2}^\pm$  at the cell interface from the cell  
 340 averages  $\bar{q}_j$  will generally result in a discontinuity in these quantities at the cell interface.

341 The flux of material across the interface of a cell is estimated by solving the local  
 342 Riemann problem, defined by the initial value problem

$$343 \quad \bar{q}(x_{j+1/2}) = \begin{cases} q_{j+1/2}^+ & \text{if } x < x_{j+1/2} \\ q_{j+1/2}^- & \text{if } x > x_{j+1/2}. \end{cases}$$

345 The numerical approximation of the physical flux across the boundary of cell,  $F_{j+1/2}$  is  
 346 given by the explicit upwind central scheme proposed by Kurganov *et al.* (Kurganov et al.  
 347 2002) as

$$348 \quad F_{j+1/2} = \frac{a_{j+1/2}^+ f(q_{j+1/2}^-) - a_{j+1/2}^- f(q_{j+1/2}^+)}{a_{j+1/2}^+ - a_{j+1/2}^-} + \frac{a_{j+1/2}^+ a_{j+1/2}^-}{a_{j+1/2}^+ - a_{j+1/2}^-} [q_{j+1/2}^+ - q_{j+1/2}^-]. \quad (22)$$

350 where the spatial derivatives in the second component of the flux term, (12c) are evaluated  
 351 using first-order upwind differencing, so that

$$352 \quad f(G_{j+1/2}^+) = (\bar{u}G)_{j+1/2}^+ + \frac{gh_{j+1/2}^+}{2} - \frac{2h_{j+1/2}^+}{3\Delta x^2} (u_{j+3/2}^+ - u_{j+1/2}^+)^2 \quad (23a)$$

$$355 \quad f(G_{j+1/2}^-) = (\bar{u}G)_{j+1/2}^- + \frac{gh_{j+1/2}^-}{2} - \frac{2h_{j+1/2}^-}{3\Delta x^2} (u_{j+1/2}^- - u_{j-1/2}^-)^2 \quad (23b)$$

357 and for the first component of the flux term, it is simply;  $f(h_{j+1/2}^\pm) = (\bar{u}h)_{j+1/2}^\pm$ .

358 At the interface of a cell,  $x_{j\pm 1/2}$  a discontinuity in the state variable will propagate with  
 359 right- and left-sided local speeds, which are estimated by

$$360 \quad a_{j+1/2}^+ = \max [\lambda_2(q_{j+1/2}^-), \lambda_2(q_{j+1/2}^+), 0],$$

362 and

$$363 \quad a_{j+1/2}^- = \min [\lambda_1(q_{j+1/2}^-), \lambda_1(q_{j+1/2}^+), 0]$$

365 where  $\lambda_1$  and  $\lambda_2$  are estimates of the smallest and largest eigenvalues, respectively of the  
 366 Jacobian  $\partial f(\mathbf{u})/\partial \mathbf{u}$  which correspond to the phase speeds. This is a common feature of  
 367 this and other exact Riemann or approximate Riemann solvers. The wave speeds or an  
 368 estimate of the wave speed is required (see, for example Zoppou and Roberts (Zoppou and  
 369 Roberts 2003)).

370 *Propagation Speeds of a Local Shock*

371 As the wave number approaches infinity,  $k \rightarrow \infty$ , from (17) the phase and group speeds  
372 of the Serre equations,  $v_p \rightarrow v_g \rightarrow u_0 \pm \sqrt{gh_0}$ , are equal to the phase speed of shallow  
373 water waves. Indeed the phase speed for the Serre equations are bounded

374                   
$$u_0 - \sqrt{gh_0} \leq u_0 \pm \sqrt{gh_0} \sqrt{\frac{3}{k^2 h^2 + 3}} \leq u_0 + \sqrt{gh_0}$$
  
375

376 by the phase speed of the shallow water wave equations. We now have an estimate of  
377 the maximum and minimum shock speed required by our chosen approximate Riemann  
378 solver.

379 **Strong-Stability-Preserving Runge-Kutta Scheme**

380 Time integration of the semi-discrete system (19) is performed using a second-order  
381 Strong Stability Preserving (SSP) Runge-Kutta scheme. Strong stability preserving schemes  
382 involve a convex combination of first-order forward Euler steps that preserve the desirable  
383 Total Variational Diminishing (TVD) properties of the Euler scheme (Shu and Osher 1988;  
384 Gottlieb et al. 2009).

385 A second-order two-stage strong stability preserving Runge-Kutta scheme is given by  
386 (Shu and Osher 1988; MacDonald et al. 2008)

387                   
$$\bar{q}^{(1)} = \bar{q}^n - \Delta t \mathcal{L}(t_n, \bar{q}^n), \quad (25a)$$
  
388

389                   
$$\bar{q}^{(2)} = \bar{q}^{(1)} - \Delta t \mathcal{L}(t_{n+1}, \bar{q}^{(1)}), \quad (25b)$$

392 and

393                   
$$\bar{q}^{n+1} = \frac{1}{2} \bar{q}^n + \frac{1}{2} \bar{q}^{(2)}. \quad (25c)$$
  
394

395

396 **Solution Process**

397 The solution of the Serre equations involves the following steps

$$\begin{aligned}
 & 398 \quad \underbrace{\left[ \begin{array}{c} h \\ G \end{array} \right]^n}_{\textcircled{1}} \xrightarrow{\mathcal{A}} \bar{u}^n \rightarrow \underbrace{\left[ \begin{array}{c} h \\ G \end{array} \right]^{(1)}}_{\textcircled{2} \text{ First Euler Step}} = \left[ \begin{array}{c} h \\ G \end{array} \right]^n - \Delta t \mathcal{L} \left[ \begin{array}{c} h \\ G \end{array} \right]^n \\
 & 399 \quad \underbrace{\left[ \begin{array}{c} h \\ G \end{array} \right]^{(1)} \xrightarrow{\mathcal{A}} \bar{u}^{(1)}}_{\textcircled{3}} \rightarrow \underbrace{\left[ \begin{array}{c} h \\ G \end{array} \right]^{(2)}}_{\textcircled{4} \text{ Second Euler Step}} = \left[ \begin{array}{c} h \\ G \end{array} \right]^{(1)} - \Delta t \mathcal{L} \left[ \begin{array}{c} h \\ G \end{array} \right]^{(1)} \\
 & 400 \quad \underbrace{\left[ \begin{array}{c} h \\ G \end{array} \right]^{n+1}}_{\textcircled{5} \text{ Average Step}} = \frac{1}{2} \left[ \begin{array}{c} h \\ G \end{array} \right]^n + \frac{1}{2} \left[ \begin{array}{c} h \\ G \end{array} \right]^{(2)}
 \end{aligned}$$

402 Step 1: Given  $h$  and  $G$ , the remaining primitive variable  $\bar{u}$  is obtained by solving the  
403 second-order elliptic equation, (10) using finite differences.

404 Step 2: Perform the reconstruction and solve the local Riemann problem to obtain the flux  
405  $F_{j\pm 1/2}$  of material across a cell interface. Evolve the solution using a first-order Euler time  
406 integration for the conserved quantities,  $h$  and  $G$ .

407 Steps 3 and 4: Repeat the process with the intermediate values and evolve using another  
408 first-order Euler step.

409 Step 5: The solution at the next time level is obtained by averaging the initial values and  
410 the values obtained from the second Euler step, which completes the second-order strong  
411 stability preserving Runge-Kutta time integration, (25).

412 The operator  $\bar{u} = \mathcal{A}[h, G]$  is the solution of the second-order elliptic equation, (10).

413 Using second-order central differences, then (10) can be written as

$$414 \quad G_j = a_j \bar{u}_{j+1} + b_j \bar{u}_j + c_j \bar{u}_{j-1} \quad (26)$$

416 where,  $a_j = -h_j^2(h_{j+1} - h_{j-1})/(4\Delta x^2) - h_j^3/(3\Delta x^2)$ ,  $b_j = h_j + 2h_j^3/(3\Delta x^2)$ , and  $c_j = h_j^2(h_{j+1} -$   
417  $h_{j-1})/(4\Delta x^2) - h_j^3/(3\Delta x^2)$  which results in a tri-diagonal system of equations which can  
418 be solved efficiently using direct methods for  $\bar{u}_j$  given  $G_j$  and  $h_j$  for all the computational  
419 nodes  $j = 1, \dots, m$ .

420 With this approach  $h$  and  $G$  can be discontinuous, which is handled by the finite volume  
421 method and approximate Riemann solver efficiently. An attractive feature of this approach  
422 is that even if  $G$  is discontinuous,  $\bar{u}$  will always be smooth.

423 The resulting numerical scheme is theoretically  $O(\Delta x^2, \Delta t^2)$  accurate. However, there  
424 is a restriction on the computational time-step that can be used in all explicit schemes.

425 Stability is satisfied when the time step  $\Delta t$  satisfies the *Courant-Friedrichs-Lowy*, (CFL)  
 426 criteria (A. Harten 1983)

$$427 \quad \Delta t < \frac{\Delta x}{2\max(|\lambda_i|)} \quad \forall i \\ 428$$

429 where  $\lambda_i$  is the  $i$ th eigenvalue of the Jacobian of the flux vector.

### 430 Convergence Rate

431 Convergence rate of the proposed schemes is determined using a known analytical  
 432 solution to the Serre equations.

433 The propagation of solitons is a common test for Boussinesq-type equations. The  
 434 Serre equations, (6) has the following analytical solution (El et al. 2006)(see, also Carter  
 435 and Cienfuegos 2011 and Chazel et al. 2011)

$$436 \quad h(x, t) = a_0 + a_1 \operatorname{sech}^2(\kappa(x - ct)) \quad (27a) \\ 437$$

438 and

$$439 \quad \bar{u}(x, t) = c \left( \frac{h(x, t) - a_0}{h(x, t)} \right) \quad (27b) \\ 440$$

441 with

$$442 \quad \kappa = \frac{\sqrt{3a_1}}{2a_0 \sqrt{a_0 + a_1}} \\ 443$$

444 and

$$445 \quad c = \sqrt{g(a_0 + a_1)}$$

447 which a solitary wave solution known as Rayleigh solitary waves. Since solitary waves  
 448 propagate at constant speed without deformation, there is a balance between nonlinear and  
 449 dispersive effects, resulting in waves that do no change with time. A numerical scheme  
 450 must accurately model the equilibrium between amplitude and frequency dispersion in  
 451 order to simulate the propagation of the wave profile at constant shape and speed. A  
 452 poorly balanced schemes and truncation errors in the numerical approximations will result  
 453 in the simulation of trailing edge dispersion waves which cause a reduction in wave height  
 454 and celerity of the predicted waves.

455 A solitary wave predicted by (27) with,  $a_0 = 10\text{m}$ ,  $a_1 = 1.0\text{m}$  and  $k = 1$ , has an  
 456 amplitude of 1.0m in a fluid that is 10m deep, with a celerity,  $c = 10.387974\text{m/s}$  and  
 457  $\kappa = 0.026112/\text{m}$ .

458 The boundary conditions imposed on the model are maintaining a water depth of 10m  
 459 with zero velocity at the upstream and downstream boundaries. The domain is 2000m  
 460 in length which is subdivided into equal increments  $\Delta x = 2\text{m}$  in length,  $\theta = 1.2$  and  
 461 the computational time step is chosen to satisfy  $Cr = \sqrt{ga_0}\Delta t/\Delta x = 0.2$ . Using these  
 462 parameters, the initial soliton profile and velocity, the analytical and the simulated water  
 463 depth and velocity at  $t = 100\text{s}$  is shown in Figure 2 for the solution of the Serre equations  
 464 written in conservation law form, (12). The numerical scheme has not produced trailing  
 465 waves in the solution, the soliton amplitude is accurately predicted and the soliton speed  
 466 is captured correctly.

467 The results from a numerical scheme are compared to the corresponding analytical  
 468 solution by using the non-dimensionless  $L_1$  norm

$$L_1 = \frac{\sum_{j=1}^m |h_j - h(x_j)|}{\sum_{j=1}^m |h(x_j)|} \quad (29)$$

471 written for  $h$  where,  $h_j$  is the simulated values of  $h(x, t)$  at  $x_j$ , and  $h(x_j)$  is the corresponding  
 472 analytical solution. The  $L_1$  norm is calculated using all the computational nodes,  $j =$   
 473  $1, \dots, m$ .

474 Performing the simulation for a range of  $\Delta x$  and keeping  $Cr = 0.2$ , the  $L_1$  norm be-  
 475 tween the simulated and analytical solution was calculated for the water depth and fluid  
 476 velocity. Plotting the  $\log_{10} L_1$  against  $\log_{10} \Delta x$  reveals that the proposed second-order strat-  
 477 egy for solving the Serre equations is second-order accurate, see Figure 3.

478 Clearly, for the simulation of the smooth soliton problem, the second-order schemes is  
 479 capable of predicting the soliton speed and its amplitude.

## 480 NUMERICAL SIMULATIONS

481 Data from two laboratory experiments are used to validate the proposed model and the  
 482 simulation of the dam-break problem is used to show that the model is stable for simulating  
 483 a wide range of discontinuous flow problems. In addition, the results from the proposed  
 484 model are compared to the results from the solution of the shallow water wave equations.  
 485 Recalling that the shallow water wave equations ignore all the dispersive terms in the Serre  
 486 equations, this comparison will reveal the importance of including the dispersive terms in  
 487 the equations. The same numerical scheme and parameters are used when solving the  
 488 Serre and shallow water wave equations. The only difference is that the Serre equations  
 489 include the dispersive terms.

## 490 Labratory Experiments

491 The frictionless horizontal flume experiment from Hammack and Segur (1978), in-  
 492 volving a negative amplitude rectangular wave and the more recent surge propagation

493 experiment conducted by Chanson (2009) are used to validate the proposed modelling ap-  
494 proach. Both produce highly dispersive waves from a discontinuous abrupt change in the  
495 initial flow conditions. In these experiments the non-hydrostatic terms cannot be neglected  
496 in the momentum equation. This is illustrated by comparing the solution of the nonlinear  
497 shallow water wave equations and the experimental data.

498 The shallow water wave equations are solved using the second-order upwind central  
499 scheme with the generalized limiter and second-order strong stability preserving Runge-  
500 Kutta scheme. The Serre equations is solved using the second-order scheme described in  
501 Section 5 with the generalized limiter.

502 *Undular Bore*

503 An undular bore was created in a large tilting flume at the Civil Engineering Depart-  
504 ment, University of Queensland. The channel is 0.5m wide, 12m in length and the undular  
505 bore was created in the horizontal flume, which has a smooth PVC bed and glass walls. A  
506 radial gate located at the downstream end of the flume,  $x = 11.9\text{m}$  controls the water depth  
507 in the flume. The radial gate is used during the experiments to produce steady subcritical  
508 flow in the flume which remains constant for the duration of the experiment. Steady flow  
509 condition are established for 15 minutes prior to an experiment. Adjacent to the radial gate  
510 is a rapidly closing Tainter gate at,  $x = 11.15\text{m}$  that spans the full width of the flume. An  
511 undular bore is generated by the rapid closure of the Tainter gate, which is estimated to  
512 take less than 0.2s, when water accumulates at the Tainter gate forming an upstream pro-  
513 gressing undular bore. The experiment ceases when the bore reaches the intake structure  
514 to avoid any interference from wave reflection. Acoustic displacement meters, located at  
515 the flume centerline at;  $x = 10.8, 8.0, 6.0, 5.0, 4.55, 4.0$  and  $3.0\text{m}$  record the progress of  
516 the bore and dispersive waves with time. Data acquisition starts 30 seconds prior to the  
517 closure of the Tainter gate.

518 The boundary conditions imposed in all the models are; at the upstream boundary,  
519  $h(0, t) = 0.192\text{m}$  and  $\bar{u}(0, t) = 0.199\text{m}^3/\text{s}$  and at the downstream Tainter gate,  $h(11.15, t) =$   
520  $0.22\text{m}$  and  $\bar{u}(11.5, t) = 0\text{m}/\text{s}$ . In all the simulations,  $\Delta x = 0.01115\text{m}$  and  $Cr = 0.2$  and the  
521 generalized minmod limiter with  $\theta = 1.2$  was used.

522 The recorded water surface profile at the acoustic displacement meters over time are  
523 shown in Figure 4 along with the simulated water surface profile predicted by the shallow  
524 water wave equations. The progress of the bore is accurately predicted by the shallow  
525 water wave equations. The lack of dispersion terms in the shallow water wave equations  
526 has meant that there are no trailing dispersive waves in the simulated results, the water  
527 surface remains constant, equal to the boundary values.

528 Leakage has occurred beneath the Tainter gate. This can be seen from Figure 4(g)  
529 where the water depth decreases in time. This has also affected the recorded water level at  
530  $x = 8\text{m}$ , shown in Figure 4(f). In all the other locations in the flume, the dispersive waves

531 are symmetrical about the predicted water level. For this problem, solving the shallow  
532 water wave equations is not appropriate. It has underestimated the amplitude of the first  
533 wave by approximately 50% of the mean height of the disturbance.

534 When dispersive terms have been included in the equations it is possible to produce  
535 dispersive waves in the predicted results. The results from the solution of the Serre equa-  
536 tions, shown in Figure 5 are a significant improvement over the results obtained from the  
537 solution of the shallow water wave equations. The simulated results show that the simu-  
538 lated bore speed is slightly slower than the observed bore speed and that predicted using  
539 the shallow water wave equation. This is the theoretical observation, where the group and  
540 phase speed of waves for the Serre equations are slower than for the shallow water wave  
541 equations. However, unlike the shallow water wave equation simulations, the proposed  
542 scheme has produced dispersive waves. The amplitude of the first dispersive wave is very  
543 close to the observed amplitude.

544 Nevertheless, these results show that the Serre equations provide a reasonable predic-  
545 tion for the arrival of the bore and its amplitude. In addition, it has accurately predicted the  
546 amplitude of the dispersive waves which have a slightly longer wavelength than the actual  
547 dispersive waves.

548 *Rectangular Initial Wave*

549 A wave maker consists of a rectangular piston 61cm in length at the end of a wave tank  
550 spans the full width of the tank. The tank is 31.6m in length, 61cm deep and 39.4cm wide,  
551 horizontal with vertical sides and is constructed from glass. The piston moved monotonically  
552 from its initial position, which is flush with the tank bed to its final elevation. It can  
553 be displaced vertically up or down. The upstream wall of the wave tank adjacent to the  
554 wave maker is a plane of symmetry. The length of the piston,  $b = 61\text{cm}$  represents the  
555 half-length of a hypothetical piston occupying the region  $-b < x < b$ . The symmetrical  
556 problem is simulated using the numerical schemes. A rectangular wave propagates fol-  
557 lowing a sudden downward 3cm movement of the piston. The quiescent water depth,  $h_1$  is  
558 fixed at 10cm. The water elevation is recorded at the fixed locations;  $x/h_1 = 0$ ,  $x/h_1 = 50$ ,  
559  $x/h_1 = 100$ ,  $x/h_1 = 150$ , and  $x/h_1 = 200$ , where  $x/h_1 = 0$  is the downstream edge of the  
560 piston.

561 The upstream and downstream boundary conditions remain constant at;  $h_1 = 10\text{cm}$   
562 and  $u_1 = 0\text{m/s}$ . In all the numerical schemes  $\Delta x = 0.0005\text{m}$ ,  $Cr = 0.2$ ,  $\Delta t = Cr\Delta x/\sqrt{h_1 g}$   
563 and  $\theta = 1$  in the generalized limiter. The solution is terminated at  $t = 50\text{s}$ .

564 The solution of the shallow water wave equations provides excellent resolution of the  
565 speed of the initial surge and the rarefaction wave, see Figure 6. It does not have the ability  
566 to reproduce the dispersive waves following the surge.

567 This is not the case for the solution of the Serre equation, shown in Figure 7. There  
568 is excellent agreement between the simulated and observed results. The rarefaction wave,

569 shock speed and the phase of the dispersive waves are faithfully reproduced by the numerical  
570 scheme.

571 The Serre equations is capable of reproducing the dispersive waves associated with the  
572 rectangular wave. The shallow water wave equations is incapable of modelling dispersive  
573 waves.

574 Once the wave train has been established, the amplitude of the dispersive waves are  
575 approximately one-third of the amplitude of the initial disturbance.

### 576 **Dam-break**

577 The dam-break problem is a standard test for models used to solve the shallow water  
578 wave equations, which has a known analytical solution (see, for example (Zoppou and  
579 Roberts 2003)). It has been chosen to demonstrate the flexibility of the proposed model  
580 for simulating both subcritical and supercritical problems.

581 The dam-break problem is solved using both the shallow water wave and Serre equa-  
582 tions. The simulated results have been plotted against the analytical solution to the shallow  
583 water wave equations for the dam break problem, which is used as reference data. The  
584 dam-break occurs in a frictionless rectangular channel, 1000m in length where the initial  
585 velocity of the water  $\bar{u} = 0\text{m/s}$  and the water depth upstream of the dam, which is located at  
586  $x = 500\text{m}$  is given by  $h_1$  and downstream of the dam by  $h_0$ . In all the models,  $\Delta x = 0.1\text{m}$ ,  
587  $Cr = 0.2$ ,  $\Delta t = Cr\Delta x / \sqrt{gh_1}$  and the solution is terminated at  $t = 30\text{s}$ . The generalized  
588 limiter with  $\theta = 1.2$  is used in the second-order schemes. Three cases are considered;  
589  $h_1 = 10\text{m}$  with  $h_0 = 1\text{m}$ ,  $h_1 = 10\text{m}$  with  $h_0 = 2\text{m}$  and  $h_1 = 1.8\text{m}$  with  $h_0 = 1\text{m}$ . These  
590 have as their maximum Froude numbers;  $Fr = u / \sqrt{gh} = 1.18, 0.81$  and  $0.29$  respectively,  
591 which were obtained from the analytical solution to the shallow water wave equations.  
592 The three problems involve supercritical flows, near critical flow and subcritical flows.

593 The simulated results using the shallow water wave equations and Serre equations  
594 solvers are shown in Figures 8-10. In all the simulation, solving the shallow water wave  
595 equations produces no dispersive waves. In all cases the arrival of the shock is accurately  
596 captured, as is the rarefaction fan and the shock height. The results shown in Figure  
597 10(b) are very similar to those obtained by El et al. (2006) who used a second-order Lax-  
598 Wendroff scheme to solve the Serre equations.

599 An interesting feature of the results shown in Figures 8-10 is that the oscillations are  
600 bounded. They are restricted to the minimum and maximum initial water depth. The  
601 simulated water velocity is also bounded. The Serre equations also conserve energy. Since  
602 energy for the Serre equations is uniformly bounded (Li 2006) then the solution is also  
603 bounded by the energy of the initial conditions.

604 The amplitude of these oscillatory waves are bounded by the maximum and minimum  
605 water depths. Therefore, the amplitude of these oscillations lie between these limits with  
606 the maximum potentially much greater than the shock height predicted by the shallow

607 water wave equations. These oscillations fluctuate about a water depth corresponding to  
608 the water depth predicted by the shallow water wave equations, that is the height of the  
609 advancing shock.

610 In these examples, the amplitude of the advancing shock is significantly underestimated  
611 by the shallow water wave equations. This would have a significant influence on  
612 the area inundated during a dam failure if the predictions were performed using the shallow  
613 water wave equations. The amplitude of the initial wave predicted by the Serre equations  
614 approached the maximum water depth. In all these examples, this is significantly greater  
615 than the shock height predicted by the shallow water wave equations. The wave train that  
616 follows the initial shock is not predicted by the shallow water wave equations. These dis-  
617 persive waves have been observed, for example during a tsunami. The use of the shallow  
618 water wave equations, in this case would predict the arrival time of the tsunami but not  
619 its amplitude. Therefore, the shallow water wave equations may not be appropriate for  
620 predicting the area inundated by a tsunami, nor its amplitude and waves that follow the  
621 initial wave front.

622 We found that the proposed scheme is more stable and accurate than using finite-  
623 difference scheme. It is only slightly more computationally expensive,  $\approx 60\%$  more ex-  
624 pensive than solving the shallow water wave equations because it requires the solution of  
625 the second-order elliptic equation.

626 **CONCLUSIONS**

627 The Serre equations are a system of equations that assume that the vertical motion  
628 of the fluid has an influence on the behaviour of the fluid. This assumption leads to a  
629 non-hydrostatic pressure distribution and dispersive terms in the governing equations. Hy-  
630 drostatic pressure distribution is assumed in the shallow water wave equations, which are  
631 obtained from the Serre equation by ignoring the dispersive terms. These dispersive terms  
632 include higher-order spatial derivatives as well as a mixed spatial and temporal derivative  
633 term. The mix derivative dispersive term in the nonlinear weakly dispersive Serre equa-  
634 tions is replaced by a new conserved quantity. The Serre equations, written in conservation  
635 law form are evolved using a finite volume scheme. The remaining primitive variable is  
636 obtained by solving a second-order elliptic equation. The proposed scheme for solving  
637 the Serre equations is shown to be simple to implement, stable for a range of problems in-  
638 cluding rapidly varying flows and it is only slightly more computationally expensive than  
639 solving the shallow water wave equations.

640 Using laboratory flume data and by simulating the dam-break problem, the importance  
641 of assuming a non-hydrostatic pressure distribution is demonstrated using problems that  
642 contain rapidly varying flows.

643 For smooth problems the shallow water wave equations and the Serre equations pro-  
644 duce identical results. However, for rapidly varying flows the Serre equations are capable  
645 of predicting not only the arrival of an advancing front but also its amplitude as well as  
646 the phase of the trailing waves. This is not the case for the shallow water wave equations  
647 which significantly underestimates the amplitude of the advancing front and is not capable  
648 of predicting the trailing waves. The underestimation is dependent on the problem and in  
649 some cases the amplitude of these oscillations can be as large as the initial disturbance.  
650 The ability to accurately predict the amplitude and phase of the oscillatory waves that ac-  
651 company rapidly varying flows, this is particularly important when modelling tsunamis,  
652 which are dispersive waves.

653 **ACKNOWLEDGEMENTS**

654 Professor H. Chanson, Department of Civil Engineering, University of Queensland  
655 for providing the data for the undular bore and to Dr David George, Cascades Volcano  
656 Observatory, U.S. Geological Survey for providing the rectangular wave data.

657 **REFERENCES**

- 658 A. Harten, A. (1983). "High resolution schemes for hyperbolic conservation laws." *Journal*  
659 *of Computational Physics*, 49(3), 357–393.  
660 Antunes do Carmo, A., Seabra-Santos, F. J., and Almeida, A. B. (1993). "Numerical solu-  
661 tion of the generalized serre equations with the maccormack finite-difference scheme."  
662 *International Journal for Numerical Methods in Fluids*, 16(8), 725–738.

- 663 Avilez-Valente, P. and Seabra-Santos, F. J. (2009). "A high-order petrov-galerkin finite  
 664 element method for the classical boussinesq wave model." *Internatioanal Journal for*  
 665 *Numerical Methods in Fluids*, 59(9), 969–1010.
- 666 Barthélemy, E. (2004). "Nonlinear shallow water theories for coastal waves." *Surveys in*  
 667 *Geophysics*, 25(3-4), 315–337.
- 668 Basco, D. R. (1987). "Computation of rapidly varied, unsteady, free-surface flow." *Water-*  
 669 *Resources Investigations Report 83-4284*, US Geological Survey.
- 670 Beji, S. and K. Nadaoka, K. (1996). "A formal derivation and numerical modelling of the  
 671 improved boussinesq equations for varying depth." *Ocean Engineering*, 23(8), 691–704.
- 672 Bonneton, P., Barthélemy, E., Chazel, F., Cienfuegos, R., Lannes, D., Marche, F., and  
 673 Tissier, M. (2011a). "Recent advances in serre-green naghdi modelling for wave trans-  
 674 formation, breaking and runup processes." *European Journal of Mechanics B/Fluids*,  
 675 30(6), 589–597.
- 676 Bonneton, P., Chazel, F., Lannes, D., Marche, F., and Tissier, M. (2011b). "A splitting  
 677 approach for the fully nonlinear and weakly dispersive green-naghdi model." *Journal of*  
 678 *Compuational Physics*, 230(4), 1479–1498.
- 679 Carter, J. D. and Cienfuegos, R. (2011). "Solitary and cnoidal wave solutions of the serre  
 680 equations and their stability." *European Journal of Mechanics B/Fluids*, 30(3), 259–268.
- 681 Chanson, H. (2009). "An experimental study of tidal bore propagation: The impact of  
 682 bridge piers and channel constriction." *Research Report CH74/09*, School of Civil En-  
 683 gineering, The University of Queensland. 104p.
- 684 Chazel, F., Lannes, D., and Marche, F. (2011). "Numerical simulation of strongly nonlin-  
 685 ear and dispersive waves using a green-naghdi model." *Journal of Scientific Computing*,  
 686 48(1-3), 105–116.
- 687 Dias, F. and Milewski, P. (2010). "On the fully-nonlinear shallow-water generalized serre  
 688 equations." *Physics Letters A*, 374(8), 1049–1053.
- 689 El, G., Grimshaw, R. H. J., and Smyth, N. F. (2006). "Unsteady undular bores in fully  
 690 nonlinear shallow-water theory." *Physics of Fluids*, 18(027104).
- 691 El, G. A., Grimshaw, R. H. J., and Smyth, N. F. (2008). "Asymptotic description of solitary  
 692 wave trains in fully nonlinear shallow-water theory." *Physica D*, 237(19), 2423–2435.
- 693 Erduran, K. S. (2007). "Further application of hybrid solution to another form of boussi-  
 694 nesq equations and comparisons." *International Journal for Numerical Methods in Flu-*  
 695 *ids*, 53(5), 827–849.
- 696 Erduran, K. S., Ilic, S., and Kutija, V. (2005). "Hybrid finite-volume finite-difference  
 697 scheme for the solution of boussinesq equations." *International Journal for Numerical*  
 698 *Methods in Fluids*, 49(11), 1213–1232.
- 699 Eskilsson, C. and Sherwin, S. J. (2002). "A discontinuous spectral element model for  
 700 boussinesq-type equations." *Journal of Scientific Computing*, 17(1-4), 143–152.

- 701 Gottlieb, S., Ketcheson, D. I., and Shu, C. W. (2009). "High order strong stability preserving time discretizations." *Journal of Scientific Computing*, 38(3), 251–289.
- 702 Green, A. E. and Naghdi, P. M. (1976). "A derivation of equations for wave propagation in water of variable depth." *Journal of Fluid Mechanics*, 78(2), 237–246.
- 703 Hammack, J. L. and Segur, H. (1978). "The korteweg-de vries equation and water waves. part 3. oscillatory waves." *Journal of Fluid Mechanics*, 84(2), 337–358.
- 704 Kurganov, A., Noelle, S., and Petrova, G. (2002). "Semidiscrete central-upwind schemes for hyperbolic conservation laws and hamilton-jacobi equations." *Journal of Scientific Computing, Society for Industrial and Applied Mathematics*, 23(3), 707–740.
- 705 Li, Y. A. (2006). "A shallow-water approximation to the full water wave problem." *Communications on Pure and Applied Mathematics*, 59(9), 1255–128.
- 706 MacDonald, C. B., Gottlieb, S., and Ruuth, S. J. (2008). "A numerical study of diagonally split runga-kutta methods for pdes with discontinuities." *Journal of Scientific Computing*, 36(1), 89–112.
- 707 Madsen, P. A., Murray, R., and Sørenson, O. R. (1991). "A new form of the boussinesq equations with improved linear dispersion characteristics." *Coastal Engineering*, 15(4), 371–388.
- 708 Madsen, P. A. and Sørensen, O. R. (1992). "A new form of boussinesq equations with improved linear dispersion characteristics. part ii. a slowly-varying bathymetry." *Coastal Engineering*, 18(3-4), 183–204.
- 709 Mei, C. C., Stiassnie, M., and Yue, D. K. K. (2005). "Theory and applications of ocean surface waves part 2 - nonlinear aspects." *Advanced Series on Ocean Engineering*, Vol. 23, World Scientific, Singapore.
- 710 Mitsotakis, D. E. (2009). "Boussinesq systems in two-space dimensions over a variable bottom for the generation and propagation of tsunami waves." *Mathematics and Computers in Simulation*, 80(4), 860–873.
- 711 Nwogu, O. (1993). "Alternative form of boussinesq equations for nearshore wave propagation." *Journal of Waterway, Port, Coastal, and Ocean Engineering, American Society of Civil Engineers*, 119(6), 618–638.
- 712 Roeber, V., Cheung, K. F., and Kobayashi, M. H. (2010). "Shock-capturing boussinesq-type model for nearshore wave processes." *Coastal Engineering*, 57(4), 407–423.
- 713 Seabra-Santos, F. J., Renouard, D. P., and Temerville, A. M. (1981). "Numerical and experimental study of the transformation of a solitary wave over a shelf or isolated obstacle." *Journal of Fluid Mechanics*, 176, 117–134.
- 714 Serre, F. (1953). "Contribution à l'étude des écoulements permanents et variables dans les canaux." *La Houille Blanche*, 6, 830–872.
- 715 Shi, F., Kirby, J. T., Harris, J. C., Geiman, J. D., and Grilli, S. T. (2012). "A high-order adaptive time-stepping tvd solver for boussinesq modeling of breaking waves and

- 739 coastal inundation.” *Ocean Modelling*, 43-44, 36–51.
- 740 Shiach, J. B. and Mingham, C. G. (2009). “A temporally second-order accurate godunov-  
741 type scheme for solving the extended boussinesq equations.” *Coastal Engineering*,  
742 56(1), 32–45.
- 743 Shu, C. W. and Osher, S. (1988). “Efficient implementation of essentially non-oscillatory  
744 shock-capturing schemes.” *Journal of Computational Physics*, 77(2), 439–471.
- 745 Soares-Frazão, S. and Guinot, V. (2008). “A second-order semi-implicit hybrid scheme for  
746 one-dimensional boussinesq-type waves in rectangular channels.” *International Journal  
747 for Numerical Methods in Fluids*, 58(3), 237–261.
- 748 Su, C. H. and Gardner, C. S. (1969). “Korteweg-de vries equation and generalisations. iii.  
749 derivation of the korteweg-de vries equation and burgers equation.” *Journal of Mathe-  
750 matical Physics*, 10(3), 536–539.
- 751 Tonelli, M. and Petti, M. (2009). “Hybrid finite volume-finite difference scheme for 2dh  
752 improved boussinesq equations.” *Coastal Engineering*, 56(5-6), 609–620.
- 753 Tonelli, M. and Petti, M. (2012). “Shock-capturing boussinesq model for irregular wave  
754 propagation.” *Coastal Engineering*, 61(8-19).
- 755 van Leer, B. (1979). “Towards the ultimate conservative difference scheme, v. a second-  
756 order sequel to godunov’s method.” *Journal of Computational Physics*, 32(1), 101–136.
- 757 Witting, G. B. (1984). “A unified model for the evolution of nonlinear water waves.” *Jour-  
758 nal of Computational Physics*, 56(2), 203–236.
- 759 Zoppou, C. and Roberts, S. (2003). “Explicit schemes for dam-break simulations.” *Journal  
760 of Hydraulic Engineering, American Society of Civil Engineers*, 129(1), 11–34.
- 761 Zou, Z. L. (1999). “Higher order boussinesq equations.” *Ocean Engineering*, 26(8), 767–  
762 792.

## 763 NOTATION

764 The following symbols are used in this paper:

- $A$  = amplitude of the Fourier component for the water depth (m);  
 $a_j$  = ??;  
 $a_{j\pm 1/2}^\pm$  = characteristic wave amplitude (m);  
 $b_j$  = ??;  
 $Cr$  =  $u\Delta t/\Delta x$  computational Courant number;  
 $\mathbf{F}$  = flux vector of conserved quantities;  
 $Fr$  =  $u/\sqrt{gh}$  Froude number;  
 $F_{j\pm 1/2}$  = ??;  
 $f$  = ??;  
 $f_{j\pm 1/2}$  = ??;  
 $G$  = a conserved quantity ( $\text{m}^2/\text{s}$ );

$\mathbf{g}$	$(0, g)$ (m/s <sup>2</sup> );
$g$	gravitational acceleration (m/s <sup>2</sup> );
$h$	water depth (m);
$h_0$	initial water depth downstream of a dam or characteristic water depth (m);
$h_1$	initial water depth upstream of a dam (m);
$I_j$	??;
$i$	$\sqrt{-1}$ ;
$k$	wave number;
$L$	wavelength (m);
$P_j$	??;
$p$	pressure (N/m <sup>2</sup> );
$p_a$	atmospheric pressure (N/m <sup>2</sup> );
$q$	a conserved quantity;
$\bar{q}_j$	??;
$q_{j\pm 1/2}^\pm$	??;
$r_j$	??;
$S_j$	??;
$t$	time (s);
$U$	amplitude of the Fourier component for the velocity (m/s);
$\mathbf{U}$	$(h, G)^T$ and
$\mathbf{u}$	$(u(\mathbf{x}, t), w(\mathbf{x}, t))$ (m/s);
$u$	fluid particle velocity $x$ -direction (m/s);
$\bar{u}$	depth averaged velocity (m/s);
$u_0$	initial velocity downstream of a dam (m/s);
$u_1$	initial velocity upstream of a dam (m/s);
$\vec{\mathbf{u}}$	unit vector normal to the surface;
$V_j$	??;
$v_g$	group velocity (m/s);
$v_p$	phase velocity (m/s);
$w$	fluid particle velocity $z$ -direction (m/s);
$\mathbf{x}$	$(x, z)$ (m);
$x$	horizontal coordinate direction (m);
$z$	vertical coordinate direction (m)
$z_b$	elevation of the bed (m);
$\mathcal{A}[h, G]$	operator representing the solution of a second-order elliptic equation;
$\mathcal{L}(t_n, \bar{q}^n)$	??;
$\Delta q_{j+1/2}$	$q_{j+1} - q_j$
$\Delta t$	computational time step (s);

$\Delta x$  = computational distance increment (m);  
 $\epsilon$  = nonlinearity parameter  $a/h_0$ ;  
 $\phi$  = ??;  
 $\theta$  = ?? and  
 $\rho$  = density ( $\text{kg}/\text{m}^3$ );  
 $\omega$  = frequency (rad);  
 $\xi$  = depth below the water surface (m);  
 $\mu$  = frequency dispersion  $kh$  (m); and  
 $\sigma$  = shallowness parameter  $h_0^2/L^2$ .

<sup>765</sup> **SUBSCRIPTS**

<sup>766</sup>  $i$  = eigenvalue number; and  
 $j$  = node number.

767      **List of Tables**

768            2	The major differences between the Serre and shallow water wave equa-	
769	tions describing one-dimensional unsteady flow over a frictionless hori-	
770	zontal bed. . . . .	28

**TABLE 2. The major differences between the Serre and shallow water wave equations describing one-dimensional unsteady flow over a frictionless horizontal bed.**

	Serre Equations	Shallow Water Wave Equations
Longitudinal velocity	$\bar{u}(x, t) = u(x, t)$	$\bar{u}(x, t) = \frac{1}{h} \int_0^h u(x, z, t) dz$
Vertical particle velocity	$w _z = -(z - z_b) \frac{\partial \bar{u}}{\partial x}$	$w _z = 0$
Pressure	$p _\xi = p_a + \rho g \xi + \frac{\rho}{2} \xi (2h - \xi) \left( \frac{\partial \bar{u}}{\partial x} \frac{\partial \bar{u}}{\partial x} - \bar{u} \frac{\partial^2 \bar{u}}{\partial x^2} - \frac{\partial^2 \bar{u}}{\partial x \partial t} \right)$	$p _\xi = p_a + \rho g \xi$
Continuity equation	$\frac{\partial h}{\partial t} + \frac{\partial(\bar{u}h)}{\partial x} = 0$	$\frac{\partial h}{\partial t} + \frac{\partial(\bar{u}h)}{\partial x} = 0$
Momentum equation	$\frac{\partial(\bar{u}h)}{\partial t} + \frac{\partial}{\partial x} \left[ \bar{u}^2 h + \frac{gh^2}{2} + \frac{h^3}{3} \left( \frac{\partial \bar{u}}{\partial x} \frac{\partial \bar{u}}{\partial x} - \bar{u} \frac{\partial^2 \bar{u}}{\partial x^2} - \frac{\partial^2 \bar{u}}{\partial x \partial t} \right) \right] = 0$	$\frac{\partial(\bar{u}h)}{\partial t} + \frac{\partial}{\partial x} \left( \bar{u}^2 h + \frac{gh^2}{2} \right) = 0$
Phase velocity	$v_p = \bar{u} \pm \sqrt{gh} \sqrt{\frac{3}{\mu^2 + 3}}$	$v_p = \bar{u} \pm \sqrt{gh}$
Group velocity	$v_g = \bar{u} \pm \sqrt{gh} \left( \sqrt{\frac{3}{\mu^2 + 3}} \mp \mu^2 \sqrt{\frac{3}{(\mu^2 + 3)^3}} \right)$	$v_g = \bar{u} \pm \sqrt{gh}$

771 **List of Figures**

772      1	The notation used for one-dimensional flow governed by the Serre equation.	31
773      2	The progress of a initial solitary wave, given by (27) over a horizontal bed predicted by the solution of (12) ( $\circ$ ) at $t = 100$ s with the water depth, $h(x, t)$ shown in (a) and the velocity, $\bar{u}(x, t)$ in (b) plotted against the analytical solution (—). . . . .	32
777      3	The $L_1$ convergence rate for the simulated water depth ( $\triangle$ ) and velocity ( $\square$ ) obtained from the second-order scheme solution of (12) to the solitary wave example, given by (27). . . . .	33
780      4	Measured (—) and simulated ( $\circ$ ) water depth, $h(x, t)$ for the undular bore experiment in a frictionless rectangular channel using the solution of the shallow water wave equations with the simulated (—) and measured ( $\circ$ ) results shown for (a) $x = 3$ m, (b) $x = 4$ m, (c) $x = 4.55$ m, (d) $x = 5$ m, (e) $x = 6$ m, (f) $x = 8$ m, and (g) $x = 10.8$ m. . . . .	34
785      5	Measured (—) and simulated ( $\circ$ ) water depth, $h(x, t)$ for the undular bore experiment in a frictionless rectangular channel using the solution of the Serre equations with the simulated and measured results shown for (a) $x = 3$ m, (b) $x = 4$ m, (c) $x = 4.55$ m, (d) $x = 5$ m, (e) $x = 6$ m, (f) $x = 8$ m, and (g) $x = 10.8$ m. . . . .	35
790      6	Measured (—) and simulated ( $\circ$ ) water depth, $h(x, t)$ for the rectangular wave experiment in a frictionless rectangular channel, with $h_1 = 0.1$ m, $u_1 = u_0 = 0$ m/s and $h_0 = 0.07$ m using the solution of the shallow water wave equations with the simulated and measured results shown for (a) $x/h_1 = 0$ , (b) $x/h_1 = 50$ , (c) $x/h_1 = 100$ , (d) $x/h_1 = 150$ , and (e) $x/h_1 = 200$ . . . . .	36
795      7	Measured (—) and simulated ( $\circ$ ) water depth, $h(x, t)$ for the rectangular wave experiment in a frictionless rectangular channel, with $h_1 = 0.1$ m, $u_1 = u_0 = 0$ m/s and $h_0 = 0.07$ m using the solution of the Serre equations with the simulated and measured results shown for the simulated and measured results shown for (a) $x/h_0 = 0$ , (b) $x/h_0 = 50$ , (c) $x/h_0 = 100$ , (d) $x/h_0 = 150$ , and (e) $x/h_0 = 200$ . . . . .	37
801      8	Analytical (—) solution to the shallow water wave equations and simulated ( $\circ$ ) water depth, $h(x, t)$ for the dam break problem in a frictionless rectangular channel, 1000m in length, $u_1 = u_0 = 0$ m/s, $h_1 = 10$ m and $h_0 = 1$ m using the (a) shallow water equations solver and (b) Serre equations solver at $t = 30$ s. . . . .	38

806	9	Analytical (—) solution to the shallow water wave equations and simulated (o) water depth, $h(x, t)$ for the dam-break problem in a frictionless rectangular channel, 1000m in length, $u_1 = u_0 = 0\text{m/s}$ , $h_1 = 10\text{m}$ and $h_0 = 2\text{m}$ using the (a) shallow water equations solver and (b) Serre equations solver at $t = 30\text{s}$ . . . . .	39
811	10	Analytical (—) solution to the shallow water wave equations and simulated (o) water depth, $h(x, t)$ for the dam-break problem in a frictionless rectangular channel, 1000m in length, $u_1 = u_0 = 0\text{m/s}$ , $h_1 = 1.8\text{m}$ and $h_0 = 1\text{m}$ using the (a) shallow water equations solver and (b) Serre equations solver at $t = 30\text{s}$ . . . . .	40

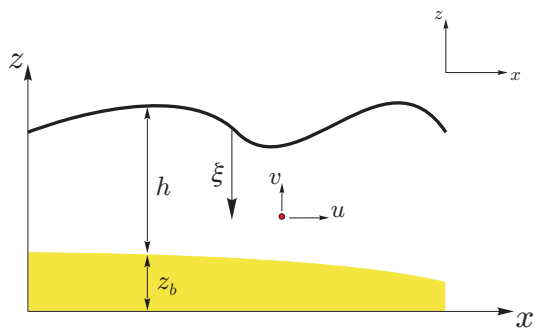


**FIG. 1. The notation used for one-dimensional flow governed by the Serre equation.**

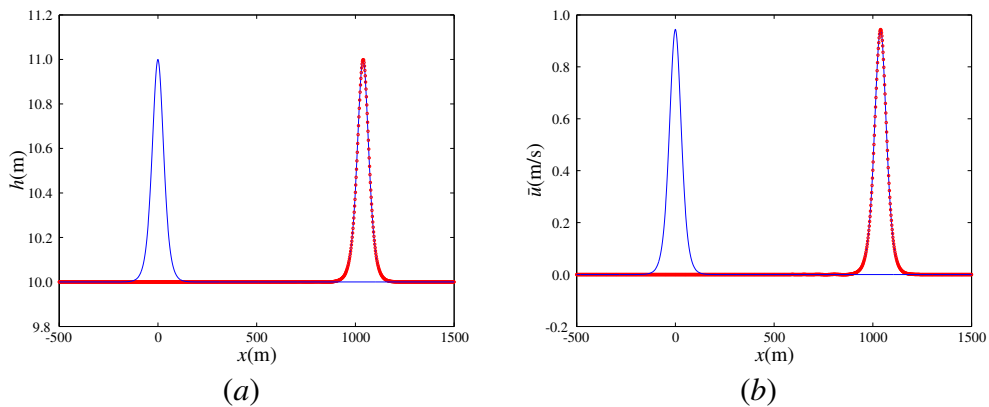


**FIG. 2. The progress of an initial solitary wave, given by (27) over a horizontal bed predicted by the solution of (12) ( $\circ$ ) at  $t = 100$ s with the water depth,  $h(x, t)$  shown in (a) and the velocity,  $\bar{u}(x, t)$  in (b) plotted against the analytical solution (—).**

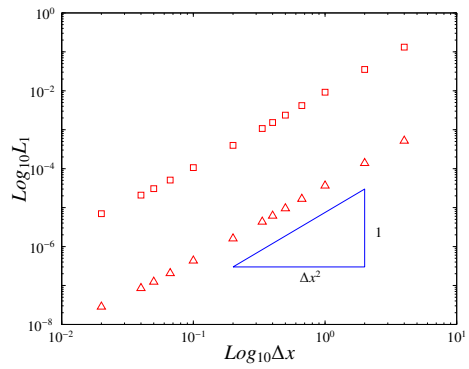


**FIG. 3. The  $L_1$  convergence rate for the simulated water depth ( $\Delta$ ) and velocity ( $\square$ ) obtained from the second-order scheme solution of (12) to the solitary wave example, given by (27).**

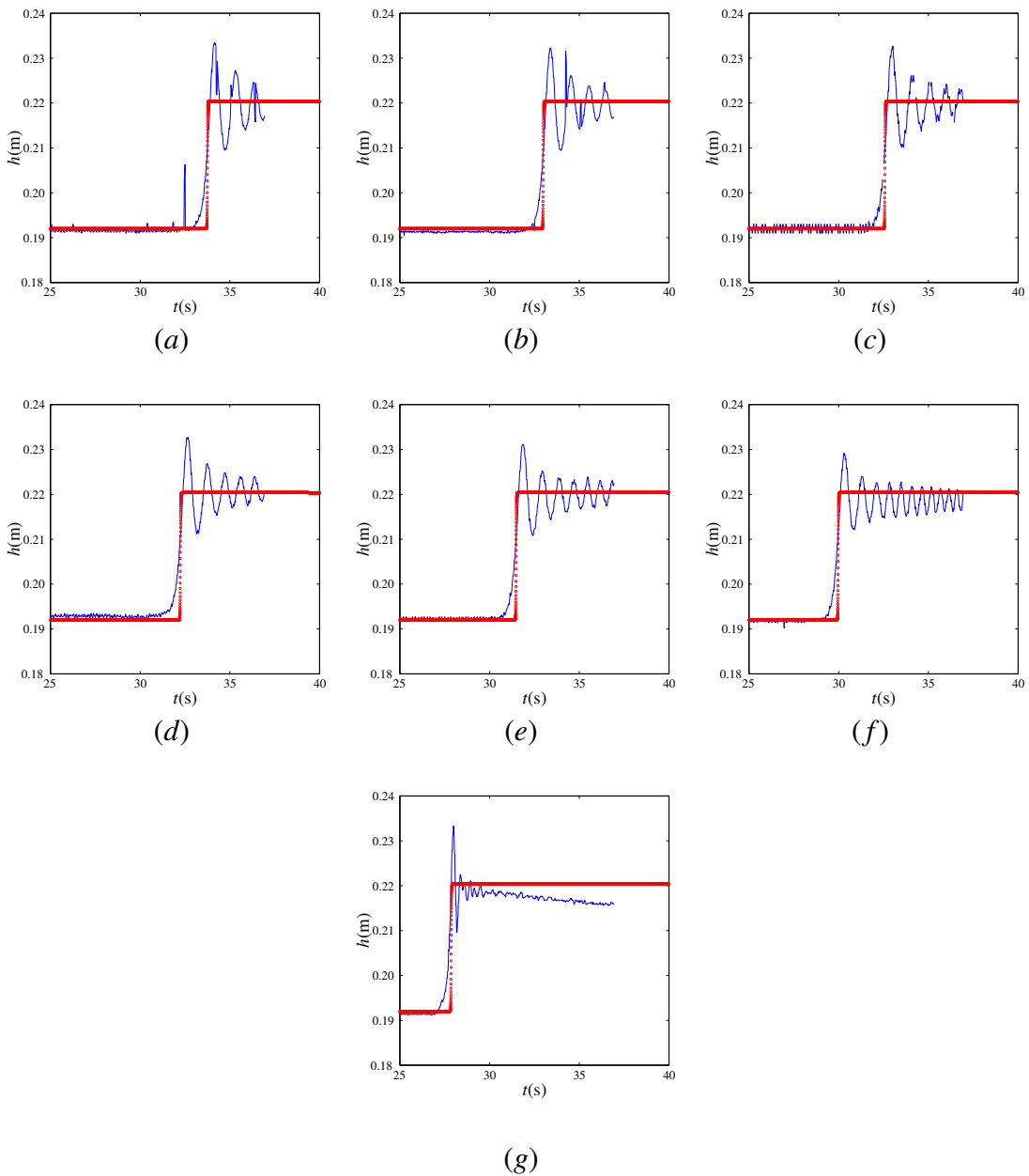


**FIG. 4. Measured (—) and simulated (○) water depth,  $h(x, t)$  for the undular bore experiment in a frictionless rectangular channel using the solution of the shallow water wave equations with the simulated (—) and measured (○) results shown for (a)  $x = 3\text{m}$ , (b)  $x = 4\text{m}$ , (c)  $x = 4.55\text{m}$ , (d)  $x = 7\text{m}$ , (e)  $x = 8\text{m}$ , and (f)  $x = 10.8\text{m}$ .**

File Name: Serre'ASCE.tex  
Date: 11/02/2015 at 12:03 Noon

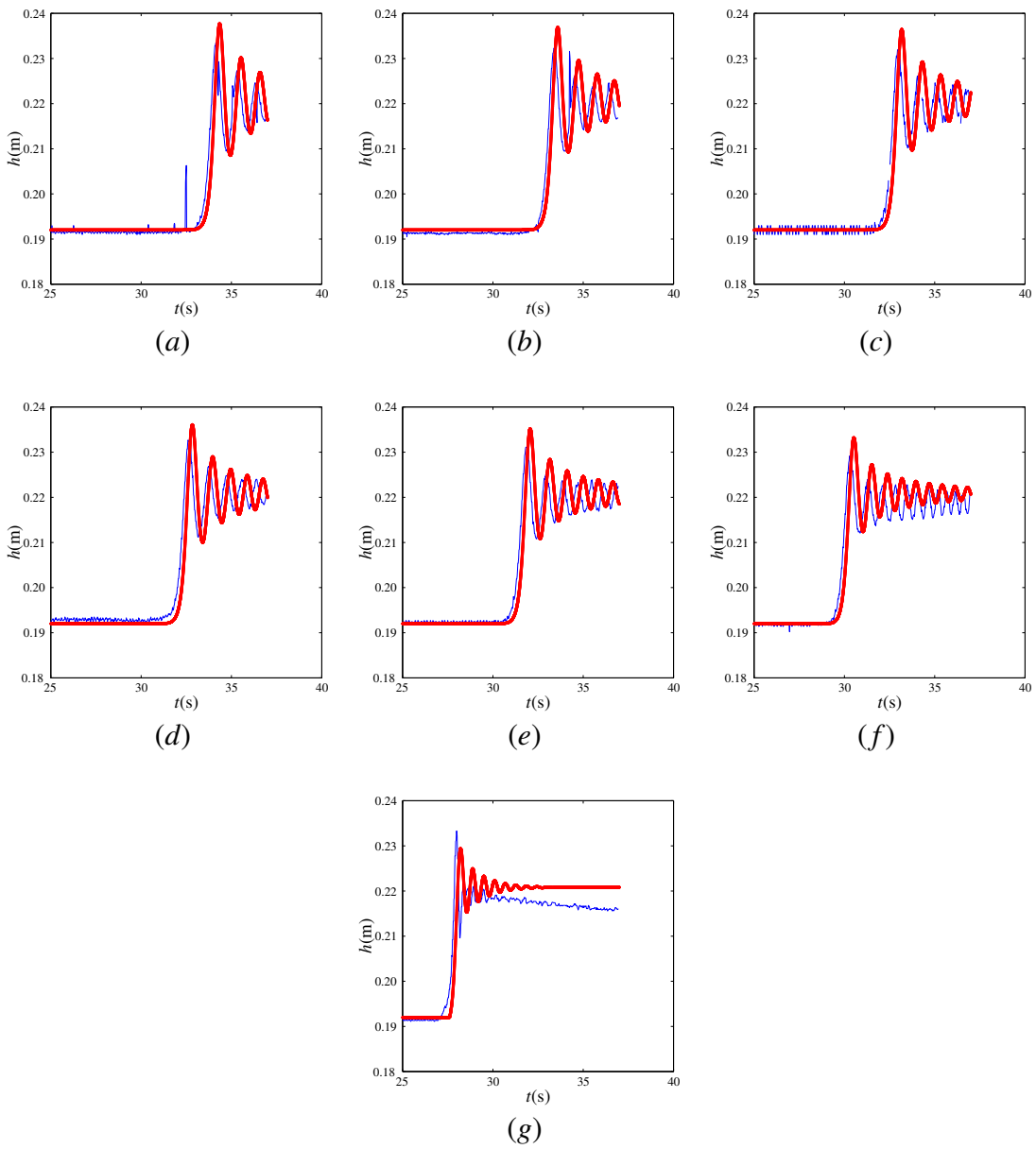


**FIG. 5. Measured (—) and simulated (○) water depth,  $h(x, t)$  for the undular bore experiment in a frictionless rectangular channel using the solution of the Serre equations with the simulated and measured results shown for (a)  $x = 3\text{m}$ , (b)  $x = 4\text{m}$ , (c)  $x = 4.55\text{m}$ , (d)  $x = 5\text{m}$ , (e)  $x = 6\text{m}$ , (f)  $x = 8\text{m}$ , and (g)  $x = 0.8\text{m}$ .**

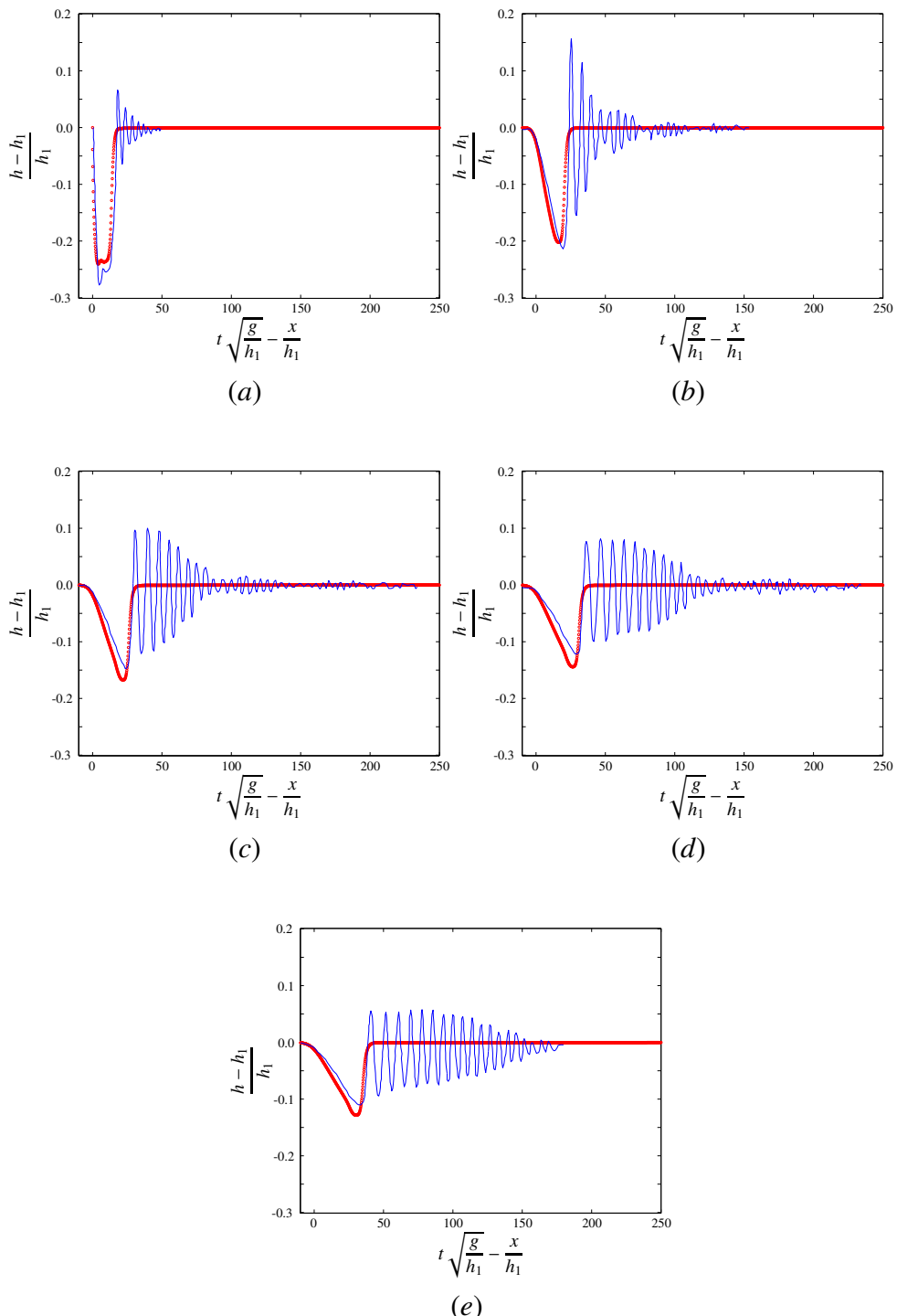


**FIG. 6. Measured (—) and simulated (○) water depth,  $h(x, t)$  for the rectangular wave experiment in a frictionless rectangular channel, with  $h_1 = 0.1\text{m}$ ,  $u_1 = u_0 = 0\text{m/s}$  and  $h_0 = 0.07\text{m}$  using the solution of the shallow water wave equations with the simulated and measured results shown for (a)  $x/h_1 = 0$ , (b)  $x/h_1 = 50$ , (c)  $x/h_1 = 100$ , (d)  $x/h_1 = 150$ , and (e)  $x/h_1 = 200$ .**

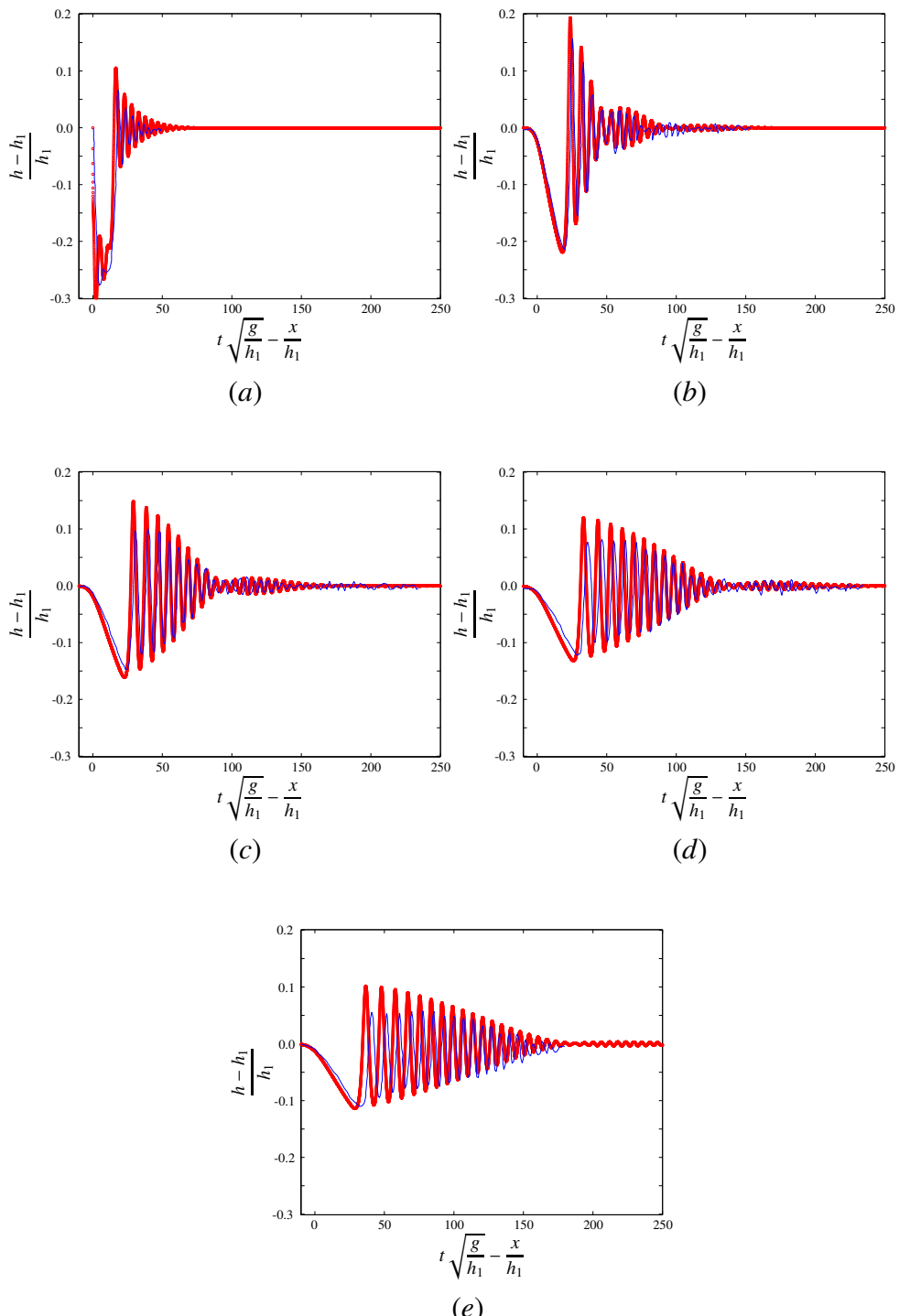


**FIG. 7. Measured (—) and simulated (○) water depth,  $h(x, t)$  for the rectangular wave experiment in a frictionless rectangular channel, with  $h_1 = 0.1\text{m}$ ,  $u_1 = u_0 = 0\text{m/s}$  and  $h_0 = 0.07\text{m}$  using the solution of the Serre equations with the simulated and measured results shown for the simulated and measured results shown for (a)  $x/h_0 = 0$ , (b)  $x/h_0 = 50$ , (c)  $x/h_0 = 100$ , (d)  $x/h_0 = 150$ , and (e)  $x/h_0 = 200$**

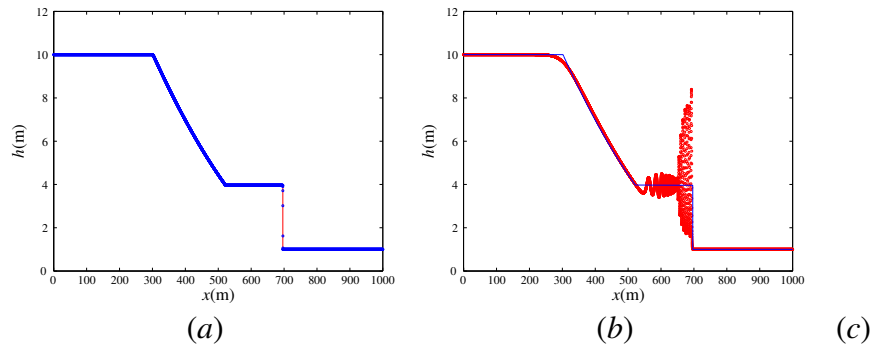


**FIG. 8. Analytical (—) solution to the shallow water wave equations and simulated (○) water depth,  $h(x, t)$  for the dam break problem in a frictionless rectangular channel, 1000m in length,  $u_1 = u_0 = 0\text{m/s}$ ,  $h_1 = 10\text{m}$  and  $h_0 = 1\text{m}$  using the (a) shallow water equations solver and (b) Serre equations solver at  $t = 30\text{s}$ .**

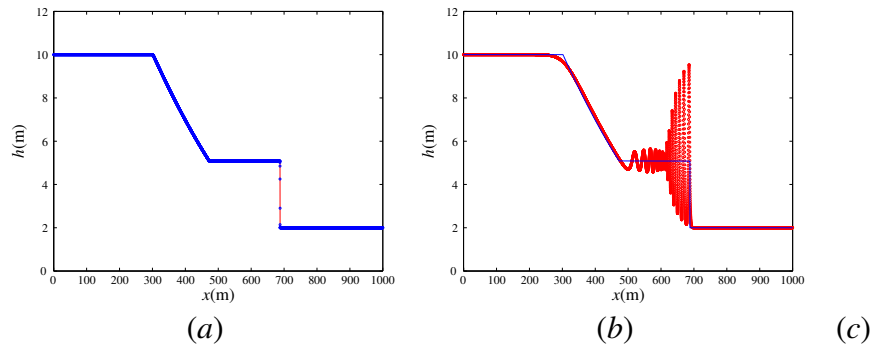


**FIG. 9. Analytical (—) solution to the shallow water wave equations and simulated (○) water depth,  $h(x, t)$  for the dam-break problem in a frictionless rectangular channel, 1000m in length,  $u_1 = u_0 = 0\text{m/s}$ ,  $h_1 = 10\text{m}$  and  $h_0 = 2\text{m}$  using the (a) shallow water equations solver and (b) Serre equations solver at  $t = 30\text{s}$ .**

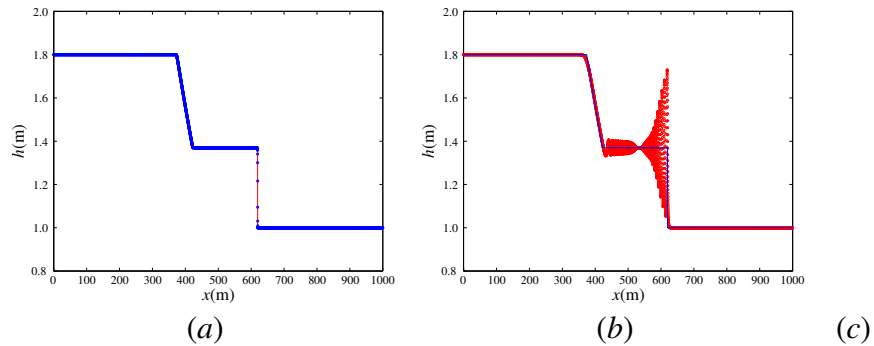


**FIG. 10.** Analytical (—) solution to the shallow water wave equations and simulated ( $\circ$ ) water depth,  $h(x, t)$  for the dam-break problem in a frictionless rectangular channel, 1000m in length,  $u_1 = u_0 = 0\text{m/s}$ ,  $h_1 = 1.8\text{m}$  and  $h_0 = 1\text{m}$  using the (a) shallow water equations solver and (b) Serre equations solver at  $t = 30\text{s}$ .